Percolation of the two-dimensional XY model in the flow representation

Bao-Zong Wang [1,*] Pengcheng Hou [1,*] Chun-Jiong Huang [2,1,†] and Youjin Deng [1,3,‡]

[1] *Hefei National Laboratory for Physical Sciences at Microscale, Department of Modern Physics, University of Science and Technology of China, Hefei 230027, China*

[2] *Department of Physics and HKU-UCAS Joint Institute for Theoretical and Computational Physics at Hong Kong, The University of Hong Kong, Hong Kong, China*

[3] *CAS Center for Excellence and Synergetic Innovation Center in Quantum Information and Quantum Physics, University of Science and Technology of China, Hefei, Anhui 230026, China*

(Received 28 October 2020; accepted 25 May 2021; published 21 June 2021)

We simulate the two-dimensional XY model in the flow representation by a worm-type algorithm, up to linear system size $L = 4096$, and study the geometric properties of the flow configurations. As the coupling strength K increases, we observe that the system undergoes a percolation transition $K_{\rm perc}$ from a disordered phase consisting of small clusters into an ordered phase containing a giant percolating cluster. Namely, in the low-temperature phase, there exhibits a long-ranged order regarding the flow connectivity, in contrast to the quasi-long-range order associated with spin properties. Near $K_{\rm perc}$, the scaling behavior of geometric observables is well described by the standard finite-size scaling ansatz for a second-order phase transition. The estimated percolation threshold $K_{\rm perc} = 1.105\,3(4)$ is close to but obviously smaller than the Berezinskii-Kosterlitz-Thouless (BKT) transition point $K_{\rm BKT} = 1.119\,3(10)$, which is determined from the magnetic susceptibility and the superfluid density. Various interesting questions arise from these unconventional observations, and their solutions would shed light on a variety of classical and quantum systems of BKT phase transitions.

DOI: 10.1103/PhysRevE.103.062131

I. INTRODUCTION

Superfluidity was first discovered in liquid helium with the frictionless flow, and then it became an important subject of persistent experimental and theoretical investigations. In three-dimensional (3D) systems, a normal-superfluid phase transition is known to be a second-order transition accompanied by a Bose-Einstein condensation (BEC) with the spontaneously breaking of a $U(1)$ symmetry. In 2D, the spontaneous-breaking continuous symmetry is forbidden by the Mermin-Wagner-Hohenberg theorem, and BEC cannot exist. Nevertheless, superfluidity is still developed through the celebrated Berezinskii-Kosterlitz-Thouless (BKT) transition [1–4] at a finite temperature, illustrating that BEC is not an essential ingredient for superfluidity.

In statistical mechanics, the 2D XY model is the simplest system of the normal-superfluid phase transition belonging to the BKT universality class. In the XY model, the superfluid density can be calculated from the helicity modulus (the spin stiffness) in the spin representation [5] or the mean-squared winding number in the flow representation [6] which is similar to the case of the Bose-Hubbard model. In 2D systems, the superfluid density suddenly jumps from zero to a universal value at the BKT point [7], and this property has been used to determine the BKT point numerically [8–14]. Besides, the magnetic susceptibility is divergent at the BKT point and in the whole superfluid phase, referred to as the critical region. By the renormalization group (RG) analysis [3], the correlation length exponentially diverges when the BKT point is approached from the high-temperature disordered phase. For finite system sizes, this exponential divergency introduces logarithmic corrections around the BKT point, and dramatically increases the difficulty for high-precision determination of the BKT point by numerical means because of the need for large system sizes and sophisticated finite-size scaling (FSS) terms. Nonetheless, recent Monte Carlo (MC) simulations can provide precise estimates for the coupling strength $K_{\rm BKT} = 1.119\,96(6)$ [11,13,15], in agreement with the high-temperature expansions [16]. It is nevertheless noted that these estimates depend on assumptions about the logarithmic finite-size corrections, and different extrapolations can lead to somewhat different values of the BKT point. For instance, it was estimated $K_{\rm BKT} = 1.119\,2(1)$ in Ref. [14], which deviates from $K_{\rm BKT} = 1.119\,96(6)$ by about seven standard error bars.

For many statistical-mechanical systems, much insight can be gained by exploring geometric properties of the systems [17–32]. For the Ising and Potts model, geometric clusters in the Fortuin-Kasteleyn bond representation have a percolation threshold coinciding with the thermodynamic phase transition, and exhibit rich fractal properties, some of which have no thermodynamic correspondence. Similar behavior is observed for the quantum transverse-field Ising model in the path-integral representation [23]. For the 2D XY model, various attempts have also been carried out. In Ref. [33], geometric clusters are constructed as collections of spins in

*These two authors contributed equally to this paper.
†chunjiong.huang@gmail.com
‡yjdeng@ustc.edu.cn

which the orientations of neighboring spins differ less than a certain angle. The percolation transitions are found to be in the standard 2D percolation universality, regardless of the coupling strength. In Ref. [34], spins are projected onto a random orientation, and geometric clusters are constructed by a Swendsen-Wang-like algorithm with an auxiliary variable. In the low-temperature phase $K > K_{\rm BKT}$, a line of percolation transitions, consistent with the BKT universality, is observed.

In this work, we study the 2D XY model on the square lattice in the flow representation, in which each bond between neighboring sites is occupied by an integer flow, and on each site, the flows obey the Kirchhoff conservation law. The XY model in the flow representation can be efficiently simulated by worm-type algorithms [35,36]. Further, the superfluid density can be calculated through the winding number and the magnetic properties can be easily measured. From FSS analysis of the superfluid density and the magnetic susceptibility, we determine the coupling strength at the BKT transition as $K_{\rm BKT} = 1.119\,3(10)$, consistent with the most precise result $K_{\rm BKT} = 1.119\,96(6)$ [13].

Given a flow configuration, we construct geometric clusters as sets of sites connected through nonzero flows, irrespective of flow directions. The emergence of superfluidity, having a nonzero winding number, requires that there exists at least a percolating geometric cluster.

From another point of view, the flow representation of the 2D XY model can be exactly mapped onto the solid-on-solid (SOS) model [37], which describes the growth of crystals on the dual lattice. The BKT transition in the 2D XY model corresponds to the roughening transition in the SOS model, of which the domain walls are the geometric clusters in the flow representation. In the deep smooth phase of the SOS model, there are only small domain walls. A naive expectation would be that the percolation transition concides with the BKT transition and some critical percolating clusters, with K-dependent fractal dimensions, emerge in the quasi-long-range-ordered (QLRO) phase for $K > K_{\rm BKT}$.

To explore percolation in these geometric clusters, we sample the mean size of the largest clusters per site c_1, which acts as the order parameter for percolation. A percolation threshold $K_{\rm perc}$ is observed. For $K < K_{\rm perc}$, there are only small geometric clusters, and c_1 quickly drops to zero as the linear system size L increases. For $K > K_{\rm perc}$, c_1 rapidly converges to a K-dependent nonzero value, suggesting the emergence of a giant cluster and thus of a long-range order. In other words, as the coupling strength K is enhanced, the 2D XY model in the flow representation undergoes a percolation transition from a disordered phase consisting of only small clusters into an ordered phase containing a giant percolating cluster. This is dramatically different from the magnetic properties of the 2D XY model, for which the system develops a QLRO phase, without breaking the U(1) symmetry, through the BKT phase transition.

The behavior of c_1 as a function of K is very similar to the order parameter for a second-order transition. To further verify this surprising observation regarding the flow connectivity, we sample the wrapping probability R, which is known to be very powerful in the study of continuous phase transitions. It is observed that R quickly approaches to 0 and 1 for $K < K_{\rm perc}$ and $K > K_{\rm perc}$, respectively, and thus has a jump from 0 to 1 at $K_{\rm perc}$ in the thermodynamic limit. Near the percolation threshold, the R values for different system sizes have approximately common intersections, which rapidly converge to $K_{\rm perc}$. Thus, the behavior of both c_1 and R implies that the percolation transition is of a second order.

Moreover, we find that, near $K_{\rm perc}$, the FSS behavior of R is well described by the standard FSS theory for a second-order transition. From the FSS analysis of R, we determine the percolation threshold $K_{\rm perc} = 1.105\,3(4)$ and the thermal renormalization exponent $y_t = 0.39(1)$. The threshold $K_{\rm perc}$ is close to but clearly smaller than $K_{\rm BKT} = 1.119\,96(6)$. In addition, the estimated exponent $y_t = 0.39(1)$ is significantly larger than zero. From the FSS behavior of c_1, we also obtain the magnetic renormalization exponent $y_h = 1.76(2)$. It is interesting to observe that the critical exponents $[y_t = 0.39(1), y_h = 1.76(2)]$ are not equal to $(y_t = 3/4, y_h = 91/48)$ for the standard 2D percolation. These unconventional observations for the 2D XY model are much different from those for the 3D XY model, where the percolation transition and the normal-superfluid transition nicely coincide, and both are the second-order phase transition [36].

The remainder of this paper is organized as follows. Section II introduces the XY model and the flow representation. Section III describes the worm algorithm and sampled quantities. In Sec. IV, the MC data are analyzed, and the results are presented. A brief discussion is given in Sec. V.

II. XY MODEL AND THE FLOW REPRESENTATION

The XY model is formulated in terms of two-dimensional, unit-length vectors $\vec{s} \equiv (\cos\theta, \sin\theta)$, residing on sites of a lattice. The reduced Hamiltonian of the XY model (already divided by k_BT, with k_B the Boltzmann constant and T the temperature) reads as

$$\mathcal{H} = -K \sum_{\langle ij \rangle} \vec{s}_i \cdot \vec{s}_j = -K \sum_{\langle ij \rangle} \cos(\theta_i - \theta_j), \tag{1}$$

where the sum is over all nearest-neighbor pairs. The partition function of Eq. (1) can be formulated as

$$\begin{aligned} Z &= \sum_{\{\vec{s}_i\}} \exp(-\mathcal{H}) = \int_0^{2\pi} \prod_{\boldsymbol{i}} \frac{d\theta_{\boldsymbol{i}}}{2\pi} \prod_{\langle \boldsymbol{ij} \rangle} \exp\left[K \cos(\theta_{\boldsymbol{i}} - \theta_{\boldsymbol{j}})\right] \\ &= \int_0^{2\pi} \prod_{\boldsymbol{i}} \frac{d\theta_{\boldsymbol{i}}}{2\pi} \prod_{\langle \boldsymbol{ij} \rangle} \left\{ \sum_{J_{\boldsymbol{ij}}=-\infty}^{+\infty} I_{J_{\boldsymbol{ij}}}(K) \exp[i J_{\boldsymbol{ij}} (\theta_{\boldsymbol{i}} - \theta_{\boldsymbol{j}})] \right\} \\ &= \sum_{\{J_{\boldsymbol{ij}}\}} \prod_{\langle \boldsymbol{ij} \rangle} I_{J_{\boldsymbol{ij}}}(K) \int_0^{2\pi} \prod_{\boldsymbol{i}} \frac{d\theta_{\boldsymbol{i}}}{2\pi} \exp(i\theta_{\boldsymbol{i}} \nabla \cdot \boldsymbol{\mathcal{J}}_{\boldsymbol{i}}) \\ &= \sum_{\{J_{CP}\}} \prod_{\langle \boldsymbol{ij} \rangle} I_{J_{\boldsymbol{ij}}}(K), \end{aligned} \tag{2}$$

where $J_{\boldsymbol{ij}} \in (-\infty, \infty)$ is the integer flow living on the lattice bond $\boldsymbol{ij}$ with $J_{\boldsymbol{ij}} = -J_{\boldsymbol{ji}}$ and the identity $\exp[K\cos(\theta)] = \sum_{J=-\infty}^{+\infty} I_J(K) \exp(iJ\theta)$ is used and $I_J(K)$ is the modified Bessel function. On each site $\boldsymbol{i}$, $\nabla \cdot \boldsymbol{\mathcal{J}}_{\boldsymbol{i}} = \sum_{\boldsymbol{j}} J_{\boldsymbol{ij}}$ is the divergence of the flows. After the spin variables are integrated out, only those flow configurations, obeying the Kirchhoff conservation law $\nabla \cdot \boldsymbol{\mathcal{J}}_{\boldsymbol{i}} = 0$ on each site, have nonzero statistical

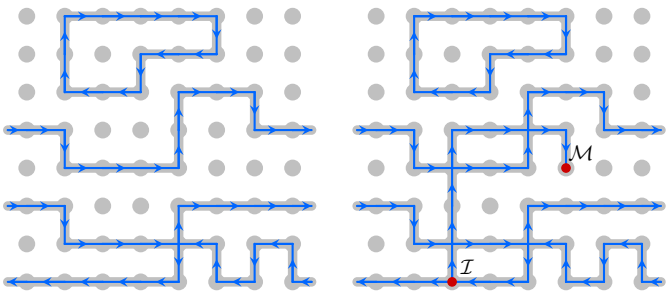

(a) a closed configuration **(b)** an open configuration

FIG. 1. Sketch of two types of flow configurations on a square lattice with periodic boundaries. Gray solid circles are the lattice sites. The blue lines with arrows represent that there is a flow on a bond. (a) A closed configuration with three clusters. The cluster, on the top, is local with winding number $\mathcal{W}_x = 0, \mathcal{W}_y = 0$ and none of the wrapping event $\mathcal{R}^{(\alpha)} = 0$. The middle cluster wraps around the x direction and has $\mathcal{W}_x \neq 0, \mathcal{R}^{(x)} = 1$. For the bottom cluster, although it also wraps around the x direction, winding numbers are zero. (b) An open configuration with two defects (red-solid circles) that do not satisfy the Kirchhoff conservation law.

weights. These flow configurations can be regarded to consist of a set of closed paths. Figure 1(a) shows an example of such configurations on the square lattice with periodic boundary conditions.

III. SIMULATION

A. Monte Carlo algorithms

The worm algorithm [35] is highly efficient for loop- or flow-type representations and is employed to simulate the XY model in this work. For worm-type simulations, the configuration space is extended to include the partition function space (the Z space) and a correlation function space (the G space). The G space can be expressed in the flow representation as well:

$$\begin{aligned} G &= \sum_{\mathcal{I}\neq\mathcal{M}} \mathcal{G}(\mathcal{I},\mathcal{M}) = \sum_{\mathcal{I}\neq\mathcal{M}} \vec{s}_{\mathcal{I}}\cdot\vec{s}_{\mathcal{M}} \exp(-\mathcal{H}) \\ &= \sum_{\mathcal{I}\neq\mathcal{M}} \int_0^{2\pi} \frac{d\theta_{\mathcal{I}}\, d\theta_{\mathcal{M}}}{(2\pi)^2} \int_0^{2\pi} \prod_i \frac{d\theta_i}{2\pi} \cosh[i(\theta_{\mathcal{I}}-\theta_{\mathcal{M}})] \\ &\quad \times \prod_{\langle ij\rangle} \exp\left[K\cos(\theta_i-\theta_j)\right] \\ &= \sum_{\mathcal{I}\neq\mathcal{M}} \int_0^{2\pi} \frac{d\theta_{\mathcal{I}}\, d\theta_{\mathcal{M}}}{(2\pi)^2} \int_0^{2\pi} \prod_i \frac{d\theta_i}{2\pi} \cosh[i(\theta_{\mathcal{I}}-\theta_{\mathcal{M}})] \\ &\quad \times \prod_{\langle ij\rangle} \left\{ \sum_{J_{ij}=-\infty}^{+\infty} I_{J_{ij}}(K) \exp[iJ_{ij}(\theta_i-\theta_j)] \right\} \\ &= \sum_{\Delta\theta=\pm1} \sum_{\{J_{ij}\}} \prod_{\langle ij\rangle} I_{J_{ij}}(K) \int_0^{2\pi} \prod_{i\neq\mathcal{I},\mathcal{M}} \frac{d\theta_i}{2\pi} \exp(i\theta_i \nabla\cdot\mathcal{J}_i) \\ &\quad \times \frac{1}{2}\int_0^{2\pi} \frac{d\theta_{\mathcal{I}}\, d\theta_{\mathcal{M}}}{(2\pi)^2} \exp\left[i\theta_{\mathcal{I}}(\nabla\cdot\mathcal{J}_{\mathcal{I}}+\Delta\theta)\right] \\ &\quad \times \exp\left[i\theta_{\mathcal{M}}(\nabla\cdot\mathcal{J}_{\mathcal{M}}-\Delta\theta)\right] \\ &= \sum_{\{J_{OP}\}} \prod_{\langle ij\rangle} I_{J_{ij}}(K). \end{aligned} \tag{3}$$

These nonzero weighted configurations $\{J_{OP}\}$ are called open configurations, in which two defects on different sites $\mathcal{I}$ and $\mathcal{M}$ are connected via an open path. An example is shown in Fig. 1(b). In the last line of the above equation, there is no $\frac{1}{2}$ because of the exchange symmetry $\mathcal{G}(\mathcal{I},\mathcal{M}) = \mathcal{G}(\mathcal{M},\mathcal{I})$. The flow configurations in the G space also obey the Kirchhoff conservation laws for each site except $\mathcal{I}$ and $\mathcal{M}$ where $\nabla\cdot\mathcal{J}_{\mathcal{I}} = -\Delta\theta$ and $\nabla\cdot\mathcal{J}_{\mathcal{M}} = \Delta\theta$, with $\Delta\theta = \pm1$. This means that there is an additional flow $+1$ from $\mathcal{I}$ to $\mathcal{M}$ or vice versa.

The partition function in the extended configuration space is

$$Z_{\text{ext}} = \omega_G Z + G, \tag{4}$$

where the relative weight ω_G between the G and the Z space can be arbitrary. For the particular choice $\omega_G = L^d$, the overall partition function becomes $Z_{\text{ext}} = \sum_{\mathcal{I},\mathcal{M}} \mathcal{G}(\mathcal{I},\mathcal{M}) = \sum_{\{\vec{s}_i\}}[(\sum_i \vec{s}_i)^2 \exp(-\mathcal{H})] = \chi Z$, where χ is the magnetic susceptibility.

The whole configuration space is specified by the flow variables as well as the positions of the pair of sites $(\mathcal{I},\mathcal{M})$. The Z space corresponds to those configurations with $\mathcal{I} = \mathcal{M}$ and this space has been expanded by $\omega_G = L^d$ times due to the defect pair $(\mathcal{I},\mathcal{M})$ locating on an arbitrary lattice site. In this formulation, one can naturally apply the following local update scheme: randomly choose $\mathcal{I}$ or $\mathcal{M}$ (say $\mathcal{I}$), move it to one of its neighboring sites (say $\mathcal{I}'$), and update the flow variable in between such that site $\mathcal{I}'$ becomes a new defect and the conservation law is recovered on site $\mathcal{I}$. Effectively, the defects $(\mathcal{I},\mathcal{M})$ experience a random walk on the lattice. The detailed balance condition reads as

$$\frac{1}{2}\frac{1}{z_d} W_\mu \mathcal{P}_{\mu\to\nu} = \frac{1}{2}\frac{1}{z_d} W_\nu \mathcal{P}_{\nu\to\mu}, \tag{5}$$

where z_d is the coordination number of the lattice and factor $1/(2z_d)$ describes the probability for choosing this particular update. Statistical weights before and after the update are accounted for by W_μ, W_ν, respectively. Taking into Eqs. (2) and (3) and the choice $\omega_G = L^d$, one has the acceptance probability according to the standard Metropolis filter as

$$P_{\text{accept}} = \min\left[1, \frac{I^\mu_{J_{ij}}(K)}{I^\nu_{J_{ij}}(K)}\right]. \tag{6}$$

The worm algorithm can be simply regarded as a local Metropolis update scheme for Z_{ext}. The superfluid density is measured in the Z space, where the two defects coincide with each other $\mathcal{I} = \mathcal{M}$. With the choice $\omega_G = L^d$, one has $Z_{\text{ext}} = \chi Z$, and the magnetic susceptibility χ as the ratio of Z_{ext} over Z. In the worm simulation, χ can be simply sampled as the statistical average of steps between subsequent closed configurations. The relative weight ω_G, of course, can take other positive value and the worm algorithm is still applicable. But weights of closed configurations W_{CP} should be scaled to $\frac{\omega_G}{L^d} W_{\text{CP}}$ in Eq. (5) and the acceptance probability needs to be modified. In this case, the worm-return time is no longer the magnetic susceptibility.

B. Sampled quantities

In the flow representation, the winding number $\mathcal{W}_\alpha$ of a closed configuration is defined as the number of flows along the spatial direction α. It can be calculated as $\mathcal{W}_\alpha = \sum_{\boldsymbol{i}} J_{\boldsymbol{i},\boldsymbol{i}+\hat{\mathbf{e}}_\alpha}$ with $\hat{\mathbf{e}}_\alpha$ being the basis vector of the direction α and sites $\boldsymbol{i}$ align on a line perpendicular to the direction α. Besides, the two-point correlations can be detected in the worm process. The magnetic susceptibility (integral of two-pint correlation) can be evaluated by the number of worm steps between subsequent hits on the Z space, known as worm-return time τ_{w}.

Given a flow configuration, we construct geometric clusters as sets of sites connected via nonzero flow variables, irrespective of the flow direction. Namely, for each pair of neighboring sites, the bond is considered to be empty (occupied) if the flow variable is zero (nonzero), and clusters are constructed in the same way as for the bond percolation model. For small K, the flow variables are mostly zeros, and the clusters are small. As K increases, the geometric clusters grow and percolate through the whole lattice via a percolation transition. Following the standard insight, we measure the following observables:

(1) The superfluid density is calculated from the squared winding number [6]

$$\rho_{\mathrm{s}} = \left\langle \mathcal{W}_x^2 + \mathcal{W}_y^2 \right\rangle / 2K, \tag{7}$$

where $\langle . \rangle$ represents the statistical average.

(2) The magnetic susceptibility $\chi = \langle \tau_{\mathrm{w}} \rangle$.

(3) The wrapping probability

$$R = \langle \mathcal{R} \rangle, \tag{8}$$

where we set $\mathcal{R} = 1$ for the event that at least one geometric cluster wraps simultaneously in two or more (x, y, or diagonal) directions.

In the disordered phase, the geometric clusters are too small to wrap and one has $R = 0$ in the $L \to \infty$ limit. In the ordered phase with a giant percolating cluster, one has $R = 1$ asymptotically. At criticality, the asymptotic value of R takes some nontrivial number $0 < R_c < 1$. The curves of R as a function of K intersect for different system sizes L, and these intersections rapidly converge to the percolation threshold K_{perc}.

(4) The size $\mathcal{C}_1$ of the largest cluster. The mean size of the largest cluster per site $c_1 = \langle \mathcal{C}_1 \rangle / L^2$. In percolation, c_1 plays a role as the order parameter. In the thermodynamic limit, one has $c_1 = 0$ in the disordered phase and $0 < c_1 < 1$ in the ordered phase. At percolation threshold K_{perc}, it scales as $c_1 \sim L^{y_h - d}$, where y_h is the magnetic renormalization exponent and it is also equal to the fractal dimension of percolation clusters.

IV. RESULTS

We simulate the XY model on the square lattice with periodic boundary conditions, with linear system sizes in the range $16 \leqslant L \leqslant 4096$ around $K = 1.11$. Here we employ a pseudorandom number generator based on the modulo-2 addition of two independent shift registers with lengths chosen as the Mersenne exponents 127 and 9689. This generator is well tested in Ref. [38], and no biased error has been found thus far. The worm simulation for the 2D XY model exhibits no critical-slowing-down, and the integrated autocorrelation time is in O(10) sweeps or even less [35]. Nonetheless, a significant fraction of the total independent samples, 25%, is spent on the thermalization before taking measurements for simplicity. After thermalizing systems to equilibration, at least 8×10^6 independent samples are produced for each K and L.

A. BKT transition

Instead of an algebraic divergence of the correlation length $\xi(t) \sim |t|^{-\nu}$ near a second-order phase transition with ν the correlation-length critical exponent, around the BKT transition point, the correlation length $\xi(t)$ diverges exponentially as

$$\xi(t) \sim \exp\left(bt^{-\frac{1}{2}}\right), \tag{9}$$

where $t = K_{\mathrm{BKT}}/K - 1$ is the reduced temperature, and b is a nonuniversal positive constant. This type of divergence for the correlation length leads to the logarithmic correction [4,8,39,40], which brings notorious difficulties for the numerical study of the BKT transition. Even though, in recent years, the estimates of K_{BKT} have been significantly improved by extensive MC simulations [11,13,14] and by tensor network algorithms [41–43].

The most precise estimate of K_{BKT} for the 2D XY model, obtained by a large-scale MC simulation with system sizes up to $L = 65\,536$, is $K_{\mathrm{BKT}} = 1.119\,96(6)$ [13], which slightly deviates from the other MC result $K_{\mathrm{BKT}} = 1.119\,2(1)$ [14]. The complicated logarithmic corrections may be the underlying reason for the inconsistency.

We estimate the BKT transition point K_{BKT} by studying the FSS of the magnetic susceptibility χ and the superfluid density ρ_s.

1. Magnetic susceptibility

According to the RG analysis, the two-point correlation function at K_{BKT} scales as $G(r) \sim r^{-\eta}(\ln r)^{-2\hat{\eta}}$ [3,4,44]. Hence, the magnetic susceptibility χ behaves as

$$\chi \sim \int_{r<\xi} d^2 r G(r) \sim \xi^{2-\eta} (\ln \xi)^{-2\hat{\eta}}, \tag{10}$$

with the RG predictions $\eta = 1/4$ and $\hat{\eta} = -1/16$.

For finite-size systems, it is hypothesized that the divergent correlation length near criticality is cut off by the linear system size as $\xi = \alpha L$, with α a nonuniversal constant. Using the linear system size, we have $\chi \sim L^{7/4}(\ln L + C_1)^{1/8}$, where $C_1 = \ln \alpha$ is a nonuniversal constant. Together with Eq. (9), one has $\alpha L \sim \exp(bt^{-1/2})$ near K_{BKT}, and the FSS of χ can be expressed as

$$\chi(t, L) \sim L^{\frac{7}{4}} (\ln L + C_1)^{\frac{1}{8}} \widetilde{\chi}[t(\ln L + C_2)^2], \tag{11}$$

where $\widetilde{\chi}[x \equiv t(\ln L + C_2)^2]$ is an universal function and $C_2 = \ln \alpha$. Although the nonuniversal constants C_1 and C_2 do not affect the asymptotic scaling for $L \to \infty$, we find that they cannot be simply neglected in finite-size analyses of MC data.

TABLE I. Fits of the magnetic susceptibility χ for the 2D XY model.

	$L_{\min}$	χ^2/DF	$K_{\rm BKT}$	C_1	q_0	C_2	q_1	b_1	d_1
	16	70.4/67	1.119 1(6)	4.1(10)	0.811(9)	1.44(9)	−0.057 3(15)	0.005(12)	−0.02(7)
	32	62.3/58	1.119 0(6)	4.5(9)	0.808(10)	1.54(11)	−0.055 4(19)	0.000 2(20)	0.01(8)
	64	54.2/49	1.119 0(11)	4.5(17)	0.808(18)	1.58(17)	−0.055(3)	0.000 05(329)	0.04(9)
	64	54.2/51	1.118 9(3)	4.64(22)	0.807(3)	1.57(12)	−0.055(2)	0	0.05(9)
χ	128	37.6/42	1.119 2(4)	4.4(4)	0.810(5)	1.42(17)	−0.057(3)	0	−0.18(13)
	256	23.4/33	1.119 9(7)	3.5(7)	0.821(9)	0.8(3)	−0.068(6)	0	−0.79(24)
	64	54.5/52	1.118 9(3)	4.62(22)	0.807(3)	1.53(9)	−0.055 6(16)	0	0
	128	39.7/43	1.119 1(4)	4.5(4)	0.809(5)	1.61(12)	−0.054 2(20)	0	0
	256	34.3/34	1.119 3(7)	4.3(7)	0.812(9)	1.60(16)	−0.054(3)	0	0

Near $K_{\rm BKT}$, we perform least-squares fits of the χ data by the ansatz

$$\chi = L^{\frac{7}{4}}(\ln L + C_1)^{\frac{1}{8}}\Big[q_0 + \sum_{k=1}^{4} q_k \epsilon^k (\ln L + C_2)^{2k} + b_1(\ln L + C_3)^{-1} + b_2 L^{-1} + d_1\epsilon^2(\ln L + C_2)^2\Big], \quad (12)$$

where $\epsilon = K_{\rm BKT} - K$. Here we take the Taylor expansion of $\tilde{\chi}$ around $K = K_{\rm BKT}$ to the fourth order. The terms with b_1 and b_2 account for the multiplicative and addictive logarithmic corrections respectively. The term with d_1 reflects the nonlinear dependence of the scaling field on K.

As a precaution against correction-to-scaling terms that we have neglected in our chosen ansatz, we impose a lower cutoff $L \geqslant L_{\min}$ on the data points admitted in the fit, and systematically study the effect by the chi-squared test (χ^2 test) when $L_{\min}$ is increased. In general, our preferred fit for any given ansatz corresponds to the smallest $L_{\min}$ for which χ^2 divided by the number of degrees of freedom (DFs) is O(1), and for which subsequent increases in $L_{\min}$ do not cause χ^2 to drop by much more than one unit per degree of freedom. The error bars of the fitting parameters are determined by the inverse of the curvature matrix at the minimum of χ^2, according to the standard error estimation method of nonlinear curve fitting.

The results are reported in Table I. In the fits with b_1, b_2 and d_1 free, we find that b_1 is consistent with zero. Further, stable fits are also obtained with $b_1 = b_2 = 0$. It is worth noting that the fitting value of d_1 is smaller than the resolution of our fits in small L, but clearly nonzero when $L \geqslant 256$. This illustrates that the RG invariant function of the 2D XY model plays the role of thermal nonlinear scaling field, i.e., $a_1\epsilon + a_2\epsilon^2 + \cdots$ [45], in which the nonuniversal coefficient a_2 cannot be neglected.

We find that the χ data for $16 \leqslant L \leqslant 4096$ and $1.104 \leqslant K \leqslant 1.136$ are well described by Eq. (12), and we estimate the BKT transition point $K_{\rm BKT} = 1.119\,3(10)$ for the 2D XY model. Our estimate is consistent with the most precise numerical estimate $K_{\rm BKT} = 1.119\,96(6)$ [13]. The intersections, in Fig. 2, show the scaled magnetic susceptibility $\chi L^{-7/4}(\ln L + C_1)^{-1/8}$ as a function of K for several system sizes. The collapse of these curves in the inset of Fig. 2 confirms the scaling behavior in Eq. (12).

2. *Superfluid density*

In the renormalization-group analysis, the superfluid density $\rho_s^{\rm r}$ has a jump at the BKT point as the temperature decreases, and, according to the Nelson-Kosterlitz criterion [7], the size of the jump is given by

$$\lim_{\substack{K \to K_{\rm BKT}^- \\ L \to \infty}} \rho_{\rm s}^{\rm r}(K, L) = \frac{2}{\pi K_{\rm BKT}}. \quad (13)$$

In the MC study of the 2D XY model, the situation is more subtle: the size of the jump depends on how the thermodynamic limit is approached. More precisely speaking, the jump of the superfluid density $\rho_{\rm s}$, calculated from the mean-square winding number of Eq. (7), becomes $f_{\rm r}\rho_{\rm s}^{\rm r}$, where the factor $f_{\rm r}$ depends on the aspect ratio L_x/L_y, with L_x and L_y being the linear sizes along the x and y directions, respectively. For the case of $L_x = L_y$, one has $f_{\rm r} = 1 - 16\pi e^{-4\pi}$, as proved in Ref. [46].

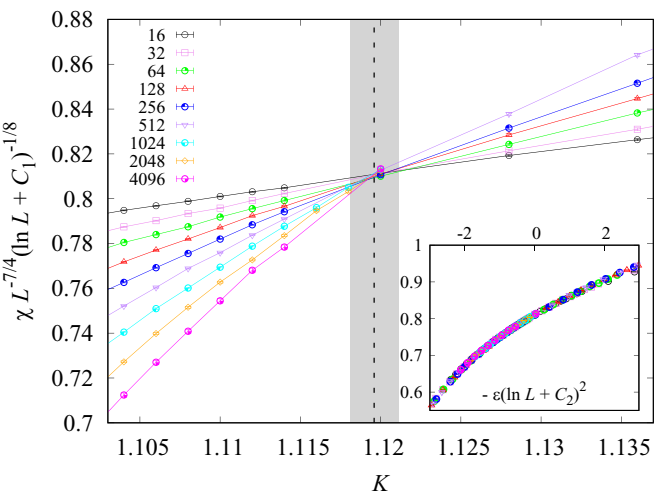

FIG. 2. Scaled magnetic susceptibility $\chi L^{-7/4}(\ln L + C_1)^{-1/8}$ versus the coupling strength K with $C_1 = 4.5$. Lines are added between the data points for clarity. The expectation value and the error bar of $K_{\rm BKT}$ are marked with the black dashed line and the gray strip, respectively. The inset shows $\chi L^{-7/4}(\ln L + C_1)^{-1/8}$ vs $-\epsilon(\ln L + C_2)^2$ with $C_2 = 1.57$. The good collapse indicates that the addictive logarithmic corrections are small, consistent with the results shown in Table I.

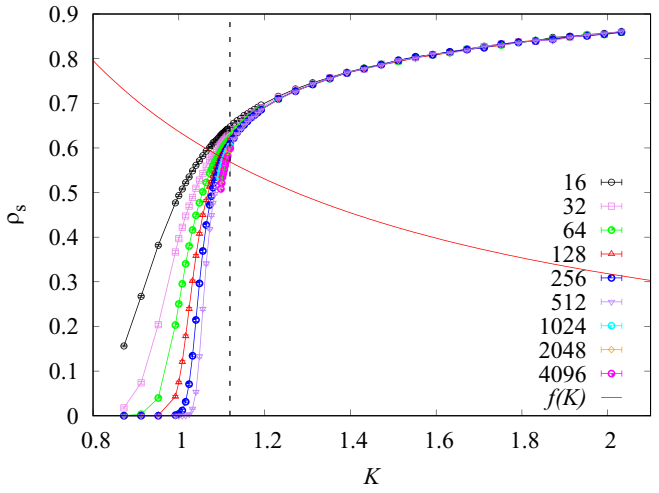

FIG. 3. Superfluid density ρ_s versus the coupling strength K. The lines connecting the data points are added for clarity. The vertical dashed line is the BKT transition coupling $K_{\rm BKT} \approx 1.1193$ (as determined in this paper) of the 2D XY model. The red line is $f(K) = 2f_r/(\pi K)$, with $f_r = 1 - 16\pi e^{-4\pi}$. The superfluid density $\rho_s(K_{\rm BKT}, L)$ will approach to the intersection of the dash line and the red line with increasing system sizes L.

The MC data for ρ_s are shown in Fig. 3, where the slow convergence of ρ_s at the BKT point is due to logarithmic corrections.

Around $K_{\rm BKT}$, we perform least-squares fits of the ρ_s data by

$$\rho_s = \rho_{s,c} + \sum_{k=1}^{3} q_k \epsilon^k (\ln L + C)^{2k} + b_1 (\ln L + C')^{-1} + b_2 L^{-1}, \tag{14}$$

where $\epsilon = K_{\rm BKT} - K$, $\rho_{s,c} = 2f_r/(\pi K_{\rm BKT})$, and the leading logarithmic correction has been taken into account. The results are summarized in Table II. With C and C' being free parameters, we have stable fits with b_1 free and $b_2 = 0$. We obtain $K_{\rm BKT} = 1.119\,3(10)$, consistent with our estimate from χ.

Similar to χ, the logarithmic corrections of ρ_s exist, and some literature achieve different estimates of the BKT point by analyzing the FSS of ρ_s [8–14], because of different forms of the logarithmic corrections.

B. Geometric properties

To have an overall picture of the geometric properties of the geometric clusters, we simulate the 2D XY model with the coupling strength in a relatively wide range $0.84 < K < 2.04$.

TABLE II. Fits of the superfluid density ρ_s for the 2D XY model.

	$L_{\rm min}$	χ^2/DFs	$K_{\rm BKT}$	C	q_1	C'	b_1
	32	23.2/55	1.119 4(4)	5.3(6)	−0.013(2)	0.25(13)	0.247(10)
ρ_s	64	21.1/47	1.119 3(6)	5.5(7)	−0.013(2)	0.2(3)	0.234(18)
	128	18.3/39	1.119 2(8)	5.3(9)	−0.013(3)	0.2(5)	0.23(3)

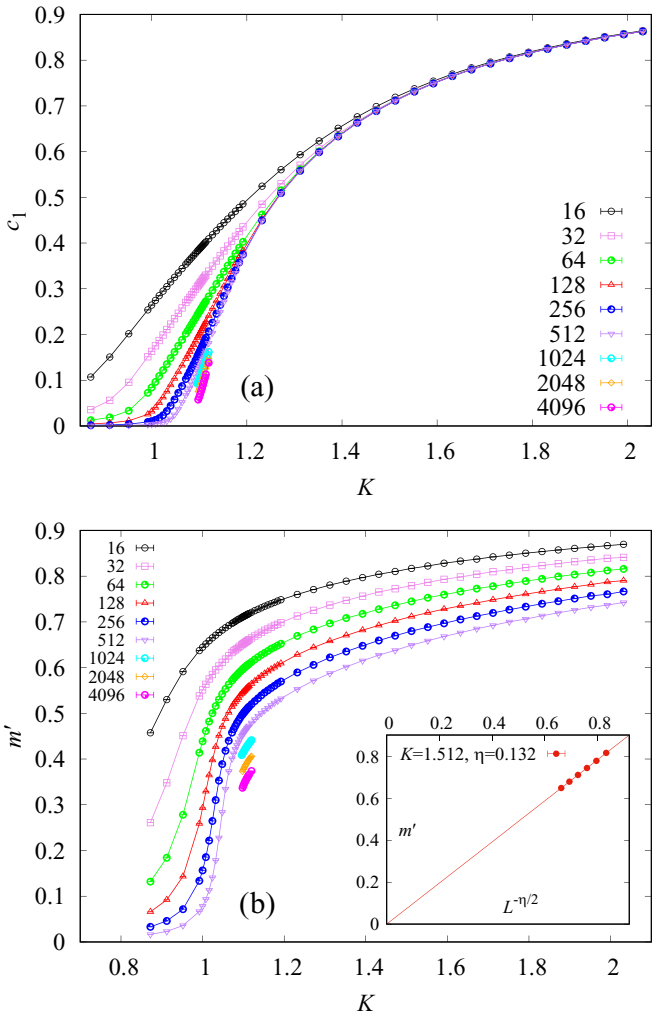

FIG. 4. Mean size of the largest cluster per site c_1 and the magnetization-density-like quantity m' versus coupling strength K. (a) c_1 vs K. The curves of different system sizes converge to a single curve in the ordered phase. (b) m' vs K. In the whole low-temperature phase, due to the absence of spontaneous symmetry breaking, m' decreases monotonically with increasing system size and reaches zero in the thermodynamic limit. As an example, the inset illustrates the algebraic decay of m' as a function of L for $K = 1.512$.

Figure 4(a) shows the mean size of the largest cluster per site c_1, which plays a role of the order parameter for percolation. The behavior of c_1 as a function of K is very similar to that for a conventional percolation transition. In the disordered phase with small K, all the geometric clusters are small and finite, and c_1 quickly drops to zero as system size L increases; in the ordered phase, a giant percolation cluster emerges, and thus a long-range order develops. For $K \geqslant 1.3$, Figure 4(a) clearly shows that c_1 rapidly converges to a nonzero value.

Figure 4(a) indicates that, for the 2D XY model, the geometric features of the flow configurations are very different from the spin properties. In the flow representation, since the spin degrees of freedom are integrated out, we cannot directly sample the magnetization density m—the order parameter for spin properties. Nevertheless, the magnetic susceptibility χ relates to m as $\chi = L^d \langle m^2 \rangle$, and we can define an effective pa-

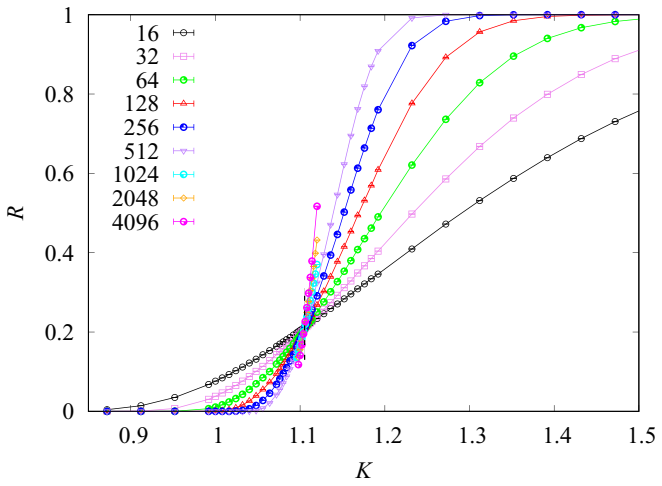

FIG. 5. Wrapping probability R versus coupling strength K.

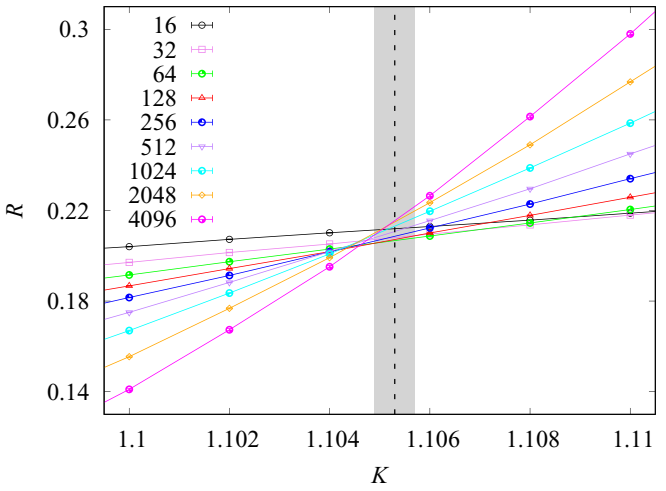

FIG. 6. Wrapping probability R versus coupling strength K around $K_{\rm perc}$. The lines connecting the data points are added for clarity. The expectation value and the error bar of $K_{\rm perc}$ are marked with the black dashed line and the gray strip, respectively.

rameter as $m' \equiv \sqrt{\chi/L^d}$. As shown in Fig. 4(b), m' also drops rapidly to zero in the disordered phase ($K < K_{\rm BKT}$), similar to c_1. However, in the low-temperature phase ($K > K_{\rm BKT}$), m' keeps decreasing as L increases, which is still clearly seen for K as large as $K \approx 2$. According to the RG analysis, the whole region for $K > K_{\rm BKT}$ is critical, one has an algebraic decay $m' \sim L^{-\eta}$ for $K > K_{\rm BKT}$, where η is a K-dependent exponent. As an illustration, the inset of Fig. 4(b) displays the algebraic decay of m' for $K = 1.152$, with $\eta \approx 0.132$.

To further demonstrate the second-order-like percolation transition of the geometric clusters, we plot in Fig. 5 the wrapping probability R versus K. In the absence or presence of a giant cluster, one expects $R \to 0$ or 1 in the $L \to \infty$ limit, respectively. This is indeed supported by Fig. 5, in which the wrapping probability R quickly converges to 1 as long as $K > 1.2$, illustrating the emergence of a giant cluster penetrating the lattice. Moreover, as for a second-order phase transition, the R curves for different system sizes have an approximately common intersection, indicating the location of the percolation threshold $K_{\rm perc}$. As L increases, the intersection of the R curves quickly approaches to $K_{\rm perc}$.

In short, the scaling behaviors of c_1 and R as a function of K are both consistent with those for a second-order phase transition, instead of a BKT transition. This is an unconventional and surprising phenomenon.

1. Percolation threshold

To have a quantitative numerical estimate of the percolation threshold $K_{\rm perc}$, we plot in Fig. 6 the MC data for the wrapping probability R near $K_{\rm perc}$. It can be seen that the uncertainty of the intersections of R for sizes $L \in [16, 4096]$ is at the third decimal place, varying in range $1.104 < K < 1.110$. As L increases, the intersection moves downward from $K \approx 1.110$ for $L \approx 32$ to $K \approx 1.104$ for $L \approx 512$, and then slightly moves upward to $K \approx 1.105$.

As in the earlier discussions, the percolation transition of the flow configurations looks like a second-order transition. Near $K_{\rm perc}$, the R data in Fig. 6 are indeed well described by the following standard FSS ansatz for a continuous phase transition

$$R(\epsilon, L) = \tilde{R}(\epsilon L^{y_t}), \tag{15}$$

where $\tilde{R}$ is a universal function and $y_t = 1/\nu$ is the thermal renormalization exponent. Taylor expansion of Eq. (15) leads to

$$R(\epsilon, L) = R_c + \sum_{k=1}^{3} q_k \epsilon^k L^{k y_t} + b_1 L^{y_i} + b_2 L^{y_i - 1} + b_3 L^{y_i - 2} + c_1 \epsilon L^{y_t + y_i} + d_1 \epsilon^2 L^{y_t}, \tag{16}$$

where $\epsilon = K - K_{\rm perc}$ and the terms with exponent $y_i < 0$ account for finite-size corrections. We fit the R data by Eq. (16), and find that the correction exponent is $y_i \approx -1$. The results with $y_i = -1$ are summarized in Table III. We obtain $K_{\rm perc} = 1.105\,3(4)$ and $y_t = 0.39(1)$, of which the error bar of $K_{\rm perc}$ is at the fourth decimal place.

Assuming that the precision of $K_{\rm perc}$ is reliable, we conclude that the percolation threshold $K_{\rm perc} = 1.105\,3(4)$ is significantly smaller than the BKT transition $K_{\rm BKT} = 1.119\,96(6)$. Actually, the deviation, at the second decimal place, can be already seen from a bare eye view of Fig. 6. Therefore, our numerical data suggest that the percolation threshold does not coincide with the BKT transition. It is noted that, since the emergence of superfluidity requests the existence of a percolating cluster, one must have $K_{\rm perc} \leqslant K_{\rm BKT}$, which is indeed satisfied in our results.

The estimated thermal exponent $y_t = 1/\nu = 0.39(1)$ is much larger than zero. If it were true, the characteristic radius of the geometric clusters would diverge as a power law $\sim \epsilon^{-\nu}$, different from the exponential growth of the correlation length near the BKT transition. This provides another piece of evidence that the percolation transition is not BKT-like. In addition, since the standard uncorrelated percolation in 2D has the thermal exponent $y_t = 3/4$, the result $y_t = 0.39(1)$ suggests that the percolation of the flow configurations is not in the 2D percolation universality class.

TABLE III. Fits of the wrapping probability R.

	$L_{\min}$	χ^2/DF	$K_{\rm perc}$	y_t	R_c	q_1	b_1	c_1	d_1
	64	60/38	1.104 95(5)	0.390(3)	0.211 2(6)	−0.62(1)	−1.9(2)	3.3(4)	−1.7(5)
R	128	32.2/31	1.105 30(9)	0.392(4)	0.217(2)	−0.61(2)	−4.6(6)	3.6(9)	−1.9(6)
	256	27.9/24	1.105 5(2)	0.393(6)	0.220(4)	−0.62(3)	−8(3)	4(2)	−1.9(7)

Further, we fit the data for the mean size of the largest cluster per site c_1 at $K = 1.106$ by the FSS ansatz

$$c_1(L) = L^{y_h-2}(a_0 + a_1 L^{y_1}), \tag{17}$$

where y_h is the magnetic exponent. The results are shown in Table IV, and we have $y_h = 1.76(2)$, smaller than $y_h = 91/48 \approx 1.89$ for the 2D percolation universality.

V. DISCUSSION

We simulate the XY model on the square lattice in the flow representation by a variant of the worm algorithm. From the FSS analysis of the magnetic susceptibility χ and the superfluid density ρ_s, we estimate the BKT transition to be $K_{\rm BKT} = 1.119\,3(10)$, consistent with the most precise result $K_{\rm BKT} = 1.119\,96(6)$.

We study the geometric properties of the flow configurations by constructing clusters as sets of sites connected through nonzero flow variables. An interesting observation is that, in the low-temperature phase, there is a giant cluster that occupies a nonzero fraction of the whole lattice, indicating the emergence of a long-range order parameter for the flow connectivity. Given a flow configuration, a nonzero winding number of flows implies a superfluid state, and can occur only if at least a geometric cluster wraps around the lattice. Such a percolating cluster can be either giant or fractal; for the latter, the cluster size per site vanishes in the thermodynamic limit. Since the low-temperature phase of the 2D XY model is a quasi-long-range-ordered state, the geometric clusters are expected to be fractal. The unexpected emergence of a giant cluster raises an important question: what is the nature of the percolation transition separating the disordered phase of small clusters and the ordered phase of a giant cluster?

The overall behaviors of the size of the largest cluster per site c_1 and of the wrapping probability R indicate that the percolation transition is of a second order. Further, the R data near the threshold $K_{\rm perc}$ are well described by a standard finite-size scaling ansatz for a continuous phase transition. From the least-squares fits of R, we obtain the percolation threshold as $K_{\rm perc} = 1.105\,3(4)$, which is close to but clearly smaller than the BKT point $K_{\rm BKT} = 1.119\,96(6)$. The thermal exponent $y_t = 1/\nu = 0.39(1)$ is also significantly larger than zero. This implies an algebraic divergence of the characteristic radius of the geometric clusters instead of an exponential growth of the correlation length near the BKT transition.

TABLE IV. Fits of the mean size of the largest cluster per site c_1.

	$L_{\min}$	χ^2/DF	y_h	a_0	a_1	y_1
	16	1.7/5	1.773(7)	0.46(5)	0.50(4)	−0.214(12)
c_1	32	1.4/4	1.768(10)	0.49(7)	0.47(6)	−0.23(3)
	64	1.0/3	1.762(13)	0.54(10)	0.44(7)	−0.25(6)

We determine the magnetic renormalization exponent as $y_h = 1.76(2)$ from the size of the largest cluster. The set of critical exponents ($y_t = 0.39(1)$, $y_h = 1.76(2)$) significantly deviates from ($y_t = 3/4$, $y_h = 91/48$) for the standard percolation in 2D. With the assumption that the estimated error margins are reliable, we obtain that the percolation transition of the geometric clusters belongs to a new universality. Caution is needed that, compared to the percolation threshold $K_{\rm perc}$, the critical exponents are more sensitive to the specific ansatz formula. Thus, there may exist some systematic errors that are not taken into account in the finally quoted errors of y_t and y_h.

Many open questions arise from these unconventional observations. First, since the difference between $K_{\rm BKT}$ and $K_{\rm perc}$ is at the second decimal place, can it be simply due to complicated logarithmic FSS corrections that have not been carefully taken into account in the analyses? If this were the case, the intersections of R for different system sizes would eventually converge to $K_{\rm BKT} \approx 1.20$. However, as shown in Fig. 6, the intersections of R are mostly in range $K \in (1.104, 1.106)$, except for some small sizes. Thus, finite-size corrections would change dramatically for $L > 4096$ if the final convergence is near $K \approx 1.20$. To clarify this point, simulation for $L \gg 4096$ is needed, which is beyond our current work. Second, what is the nature of the percolation transition for the geometric clusters? Figures 4(a) and 5 indicate that in the low-temperature

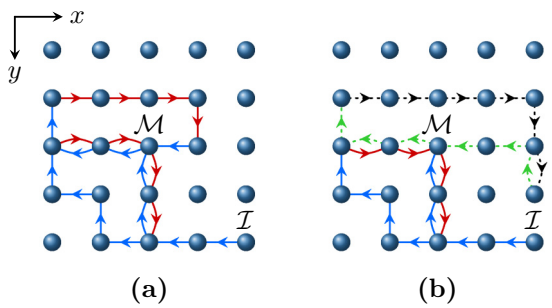

FIG. 7. (a) A typical flow configuration for the 2D XY model in representation of Eq. (A4). The red and blue lines with arrows represent a flow with J_{ij}^{+} and J_{ij}^{-} on a bond, respectively. (b) A typical flow configuration for the 2D O(4) spin model in the representation of Eq. (B6). The red solid, blue solid, black dotted, and green dotted lines with arrows represent that there is a flow with $J_{ij}^{+(1)}$, $J_{ij}^{-(1)}$, $J_{ij}^{+(2)}$ and $J_{ij}^{-(2)}$ on a bond, respectively. Integer flow variable J^{+} (J^{-}) counts along the positive (negative) direction of lines in both (a) and (b) configurations.

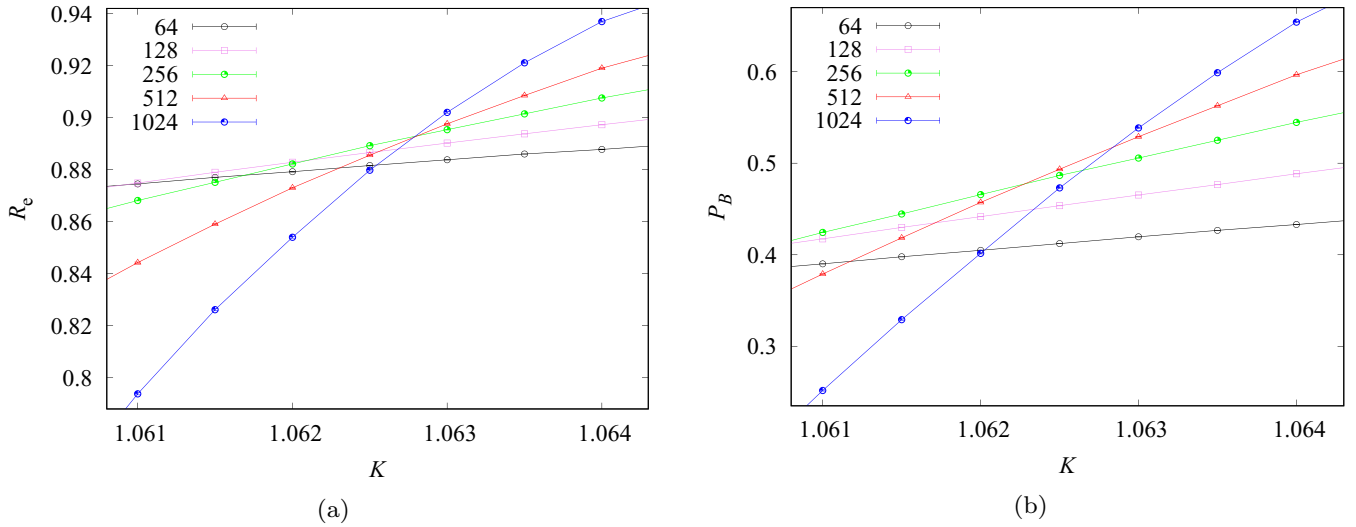

FIG. 8. Plots of R_e vs K (a) and P_B vs K (b) for the 2D XY model. The solid lines connecting data points are added for clarity.

region, a giant cluster emerges, and a long-range order parameter develops for percolation. Therefore, with the assumption that there is only one percolation transition, the disordered phase of small geometric clusters and the ordered phase of a giant cluster are expected to be separated by a second-order transition, consistent with the behaviors of c_1 and R. Third, what universality does the percolation transition belong to if it were of a second order? The estimated critical exponents ($y_t = 0.39(1)$, $y_h = 1.76(2)$) suggest that the percolation is not in the same universality as the standard percolation in 2D. Fourth, do these unconventional phenomena occur in other systems exhibiting the BKT transition?

A possible scenario is that, as the coupling strength K is enhanced, the 2D XY model in the flow representation first experiences a second-order percolation transition $K_{\rm perc}$ for the flow connectivity and then enters into the superfluidity phase via the BKT transition $K_{\rm BKT}$. In the flow configurations, the superfluid flows for $K > K_{\rm BKT}$ live on top of the giant cluster, which already appears when $K > K_{\rm perc}$. In the small intermediate region $K_{\rm BKT} > K > K_{\rm perc}$, the giant cluster, while wrapping around the lattice, is effectively built up by a set of local flow loops, and thus no superfluidity occurs.

To further verify this scenario, we explore the 2D XY model in another flow representation (Appendix A). There are two kinds of nonnegative flow variables J_{ij}^{+} and J_{ij}^{-} on each bond, representing flows along positive and negative directions. Mathematically, we can obtain the flow representation through Eq. (3) by taking a substitution $J_{ij} = J_{ij}^{+} - J_{ij}^{-}$, $\bar{J}_{ij} = \min\{J_{ij}^{+}, J_{ij}^{-}\}$ and then summing over $\bar{J}_{ij}$. At the same temperature, there will be more bonds with flows. Hence more local geometric cluster at high temperatures, and percolating clusters will form earlier with decreasing temperature in this representation. We expect the percolation threshold $K'_{\rm perc} < K_{\rm perc}$ so that the intermediate region is enlarged. Our numerical result gives $K'_{\rm perc} = 1.062\,8(2) < K_{\rm perc} < K_{\rm BKT}$, as expected.

It is proved that the percolation transition in the flow representation of the Ising model coincides with the thermodynamic phase transition in Ref. [47], while the percolation transition threshold $K_{\rm perc}$ is smaller than the BKT point. Hence, we guess that the finite-temperature percolation transition may exist in the flow representation of the 2D O(n) spin model with $n \geqslant 3$, though there is no thermodynamic or BKT transition at any finite temperature. Our numerical results of the 2D O(4) spin model (Appendix B) show that there is a percolation transition at $K = 1.888\,70(6)$ belonging to the standard 2D percolation universality class. Therefore, we reach a general conclusion: in the flow representation, whether the percolation threshold conincides with physical phase transition is model-dependent.

As for the BKT transition, there are many systems besides the 2D XY model, and the Bose-Hubbard (BH) model is a typical example of such systems. Given a finite temperature, as the on-site coupling strength is decreased, the 2D BH model undergoes a BKT phase transition from the normal fluid into the superfluid phase. Using a worm-type quantum Monte Carlo algorithm, we simulate the 2D BH model in the path-integral representation, and obtain evidence that the percolation threshold of the geometric clusters does not coincide with the BKT transition. Future works shall focus on an extensive study of low-dimensional quantum systems exhibiting the BKT phase transition.

ACKNOWLEDGMENTS

This work was supported by the National Natural Science Foundation of China (under Grant No. 11625522), the Science and Technology Committee of Shanghai (under Grant No. 20DZ2210100), and by the National Key R&D Program of China (under Grants No. 2016YFA0301604 and No. 2018YFA0306501).

APPENDIX A: XY MODEL IN ANOTHER FLOW REPRESENTATION

We consider the XY model in another different flow representation, and show stronger evidence to support our conclusion that the percolation transition in the flow configurations can be inconsistent with the BKT transition. For the

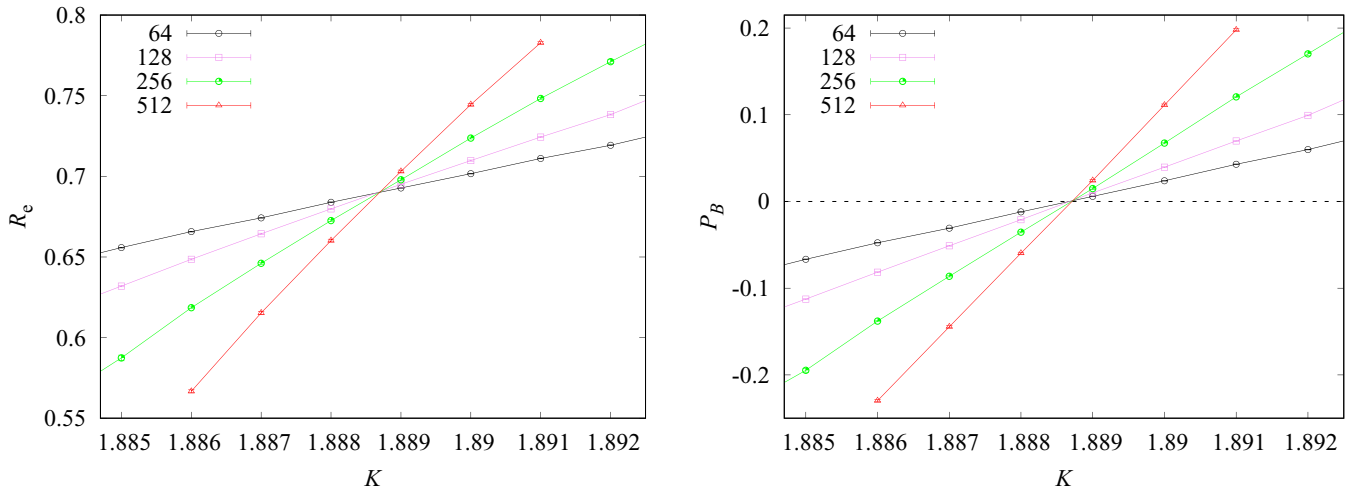

FIG. 9. Plots of R_e vs K (a) and P_B vs K (b) for the percolation model in the flow representation of the O(4) spin model. The solid lines connecting data points are added for clarity.

partition function of the XY model

$$\mathcal{Z} = \int_0^{2\pi} \prod_{\boldsymbol{i}} \frac{d\theta_i}{2\pi} \prod_{\langle \boldsymbol{ij}\rangle} e^{K\cos(\theta_i-\theta_j)}, \tag{A1}$$

we can decompose the Boltzmann statistic factor into $\exp(Ke^{i(\theta_i-\theta_j)}/2)\exp(Ke^{-i(\theta_i-\theta_j)}/2)$ and expand the exponent for each bond into Taylor series [35] as

$$e^{K\cos(\theta_i-\theta_j)} = \sum_{J_{\boldsymbol{ij}}^{\pm}=0}^{+\infty} \frac{(K/2)^{J_{\boldsymbol{ij}}^+ + J_{\boldsymbol{ij}}^-}}{J_{\boldsymbol{ij}}^+! J_{\boldsymbol{ij}}^-!} e^{i(J_{\boldsymbol{ij}}^+ - J_{\boldsymbol{ij}}^-)(\theta_i-\theta_j)}. \tag{A2}$$

Then we can rearrange terms and obtain the partition function in the flow representation as

$$\begin{aligned}\mathcal{Z} &= \sum_{\{J^+,J^-\}} \left(\prod_{\langle \boldsymbol{ij}\rangle} \frac{(K/2)^{J_{\boldsymbol{ij}}^+ + J_{\boldsymbol{ij}}^-}}{J_{\boldsymbol{ij}}^+! J_{\boldsymbol{ij}}^-!}\right) \int \prod_{\boldsymbol{i}} \frac{d\theta_i}{2\pi} e^{i\theta_i[\sum_j \mathrm{sgn}(\boldsymbol{i}\to\boldsymbol{j})(J_{\boldsymbol{ij}}^+ - J_{\boldsymbol{ij}}^-)]} \\ &= \sum_{\{J^+,J^-\}} \left(\prod_{\langle \boldsymbol{ij}\rangle} \frac{(K/2)^{J_{\boldsymbol{ij}}^+ + J_{\boldsymbol{ij}}^-}}{J_{\boldsymbol{ij}}^+! J_{\boldsymbol{ij}}^-!}\right) \\ &\quad \times \prod_{\boldsymbol{i}} \delta\left(\sum_{\boldsymbol{j}} \mathrm{sgn}(\boldsymbol{i}\to\boldsymbol{j})(J_{\boldsymbol{ij}}^+ - J_{\boldsymbol{ij}}^-)\right),\end{aligned} \tag{A3}$$

where flow variables $J_{\boldsymbol{ij}}^{\pm} \in \mathbb{N}$ represent currents flowing along positive (negative) directions, and we specify positive direction for each bond $\langle \boldsymbol{ij}\rangle$ reflected by $\mathrm{sgn}(\boldsymbol{i}\to\boldsymbol{j}) = \pm 1$. $\delta[\sum_j \mathrm{sgn}(\boldsymbol{i}\to\boldsymbol{j})(J_{\boldsymbol{ij}}^+ - J_{\boldsymbol{ij}}^-)]$ requires two currents to be conserved on each site $\boldsymbol{i}$.

For worm-type simulations, the G space can be expressed in this flow representation as well:

$$\begin{aligned}G &= \int \prod_{\boldsymbol{i}} \frac{d\theta_i}{2\pi} \cos(\theta_{\mathcal{I}} - \theta_{\mathcal{M}}) \prod_{\langle \boldsymbol{ij}\rangle} e^{K\cos(\theta_i-\theta_j)} \\ &= \sum_{\{J^+,J^-\}} \prod_{\langle \boldsymbol{ij}\rangle} \left(\frac{(K/2)^{J_{\boldsymbol{ij}}^+ + J_{\boldsymbol{ij}}^-}}{J_{\boldsymbol{ij}}^+! J_{\boldsymbol{ij}}^-!}\right) \prod_{\boldsymbol{i}} \delta\left(\sum_{\boldsymbol{j}} \mathrm{sgn}(\boldsymbol{i}\to\boldsymbol{j})(J_{\boldsymbol{ij}}^+ - J_{\boldsymbol{ij}}^-)\right. \\ &\quad \left. + \delta(\boldsymbol{i}-\mathcal{I}) - \delta(\boldsymbol{i}-\mathcal{M})\right).\end{aligned} \tag{A4}$$

In fact, the flow representation of Eq. (3) in the main text can be obtained from the representation of Eq. (A4) by taking a substitution $J_{\boldsymbol{ij}} = J_{\boldsymbol{ij}}^+ - J_{\boldsymbol{ij}}^-$, $\bar{J}_{\boldsymbol{ij}} = \min\{J_{\boldsymbol{ij}}^+, J_{\boldsymbol{ij}}^-\}$ and then summing over $\bar{J}_{\boldsymbol{ij}}$. This flow representation is shown in Fig. 7(a).

Same as the process in the main text, we construct geometric clusters as sets of sites connected via nonzero flow variables $J^{\pm}$ in the flow representation of Eq. (A4). We study

TABLE V. Fits of the wrapping probability R and the critical polynomial P_B.

	$L_{\min}$	χ^2/DF	K_{perc}	y_t	$\mathcal{O}_c$	q_1	q_2	b_1
	64	23.5/21	1.888 678(17)	0.749(5)	0.690 1(4)	−0.402(9)	−0.108(10)	−0.7(12)
R_e	128	10/13	1.888 71(4)	0.752(7)	0.691 3(12)	−0.394(14)	−0.103(12)	−14(12)
	64	23.9/22	1.888 671(12)	0.749(5)	0.689 91(14)	−0.401(9)	−0.108(10)	—
	128	11.6/14	1.888 675(15)	0.753(7)	0.690 0(3)	−0.394(14)	−0.104(12)	—
	64	23/21	1.888 693(17)	0.749(5)	−0.000 2(8)	−0.801(17)	−0.005(19)	2.5(23)
P_B	128	12.4/13	1.888 72(4)	0.752(7)	0.0018(23)	−0.79(3)	−0.007(20)	−19(23)
	64	28/23	1.888 687(7)	0.750(5)	0	−0.799(17)	−0.006(18)	—
	128	13.1/15	1.888 697(8)	0.752(7)	0	−0.79(3)	0.006(19)	—

the bond percolation model constructed by geometric clusters and its percolation transition. Here, we measure another wrapping probability R_e, namely, the probability that at least one geometric cluster wraps in any (x, y, or diagonal) direction. We find that the percolation transition exists, and the percolation threshold $K'_{\rm perc}$ is clearly smaller than the BKT transition point $K_{\rm BKT}$ and the percolation threshold $K_{\rm perc}$ determined in the flow representation of Eq. (3).

We estimate the percolation threshold $K_{\rm perc}$ by $R_{\rm e}$ and the critical polynomial $P_B(K, L) = R + R_{\rm e} - 1$. As shown in Fig. 8, the $R_{\rm e}$ and P_B curves for different systems have approximately common intersections, indicating the location of $K'_{\rm perc}$. As L increases over 256, the intersections of $R_{\rm e}$ quickly approach to $K'_{\rm perc}$. Around $K'_{\rm perc}$, we perform fits of MC data for $R_{\rm e}$ by the FSS ansatz of Eq. (16), and estimate $K'_{\rm perc} = 1.062\,8(2)$ and $y_t = 0.90(3)$.

Assuming the precision of $K_{\rm perc}$ is reliable, we find that $K'_{\rm perc} = 1.062\,8(2)$ is significantly smaller than the BKT transition point $K_{\rm BKT} = 1.119\,96(6)$ and the percolation threshold $K_{\rm perc} = 1.105\,3(4)$ determined in the original flow representation. According to our scenario, in the intermediate region $K_{\rm BKT} > K > K_{\rm perc}$, the giant cluster wrapping around the lattice can be built up by a set of local flow loops. Compared with the original representation, the local flow loops are easier to form, as shown in Fig. 7(a), so is the giant cluster. Therefore, the result for $K'_{\rm perc} < K_{\rm perc}$ seems reasonable.

APPENDIX B: O(4) SPIN MODEL IN THE FLOW REPRESENTATION

The classical O(4) spin model is formulated in terms of four-dimensional unit-length vectors $\vec{s}$, residing on sites of a lattice. Its Hamiltonian reads as

$$\mathcal{H} = -K \sum_{\langle ij \rangle} \vec{s}_i \cdot \vec{s}_j. \tag{B1}$$

Due to Polyakov's conjecture that the O(n) spin model with $n \geqslant 3$ should exhibit exponential decay of correlations in two dimensions at any positive temperature, there is no phase transition of the second-order or BKT type in the 2D O(4) spin model. However, we find that the percolation transition in the flow configurations of the 2D O(4) spin model still exists, and belongs to the 2D percolation universality.

To obtain the flow representation for the O(4) spin model, we first divide the unit spin vector $\vec{s}$ into two XY-type components:

$$\begin{aligned}\vec{s} &= \mathcal{A}^{(1)}\boldsymbol{s}^{(1)} + \mathcal{A}^{(2)}\boldsymbol{s}^{(2)} \\ &= (\cos\phi\cos\theta^{(1)}, \cos\phi\sin\theta^{(1)}, \sin\phi\cos\theta^{(2)}, \sin\phi\sin\theta^{(2)}),\end{aligned} \tag{B2}$$

where nonnegative coefficients $\mathcal{A}^{(1)} = \cos\phi$ and $\mathcal{A}^{(2)} = \sin\phi$ ($\phi \in [0, \pi/2)$), and $\boldsymbol{s}^{(\alpha)}(\alpha = 1, 2)$ is a unit-length vector on two-dimensional subspace. In this way, three degrees of freedom of the O(4) spin model are rearranged: two XY variables $\theta^{(1)}$ and $\theta^{(2)}$, and another ϕ to determine the weight difference between two XY vectors. The uniform measure for $\vec{s}$ is expressed as

$$\int d\vec{s} = \int_0^{\pi/2} d\phi \sin\phi\cos\phi \prod_{\alpha=1}^{2} \int_0^{2\pi} d\theta^{(\alpha)}. \tag{B3}$$

In addition, the Boltzmann statistical factor can be written as

$$e^{K\vec{s}_i\cdot\vec{s}_j} = \prod_{\alpha=1}^{2} e^{K_{ij}^{(\alpha)}\cos(\theta_i^{(\alpha)} - \theta_j^{(\alpha)})}, \tag{B4}$$

where we define $K_{ij}^{(\alpha)} = K\mathcal{A}_i^{(\alpha)}\mathcal{A}_j^{(\alpha)}$. Following the Taylor expansion in Eq. (A3), we can reformulate the partition function [48] as

$$Z = \sum_{\{J^{\pm(1)}\}} \sum_{\{J^{\pm(2)}\}} \prod_{\langle ij \rangle} \left(\prod_{\alpha=1}^{2} \frac{\left(K_{ij}^{(\alpha)}/2\right)^{J_{ij}^{+(\alpha)} + J_{ij}^{-(\alpha)}}}{J_{ij}^{+(\alpha)}! J_{ij}^{-(\alpha)}!} \right) \prod_i \left(\frac{\prod_\alpha \Gamma\left(\frac{\mathcal{J}_i^{(\alpha)}+2}{2}\right)}{\Gamma\left(\frac{\sum_\alpha \mathcal{J}_i^{(\alpha)}+4}{2}\right)} \prod_{\alpha=1}^{2} \delta\left(\sum_j \mathrm{sgn}(\boldsymbol{i} \to \boldsymbol{j}) \left(J_{ij}^{+(\alpha)} - J_{ij}^{-(\alpha)}\right) \right) \right), \tag{B5}$$

indicating that a graph of the 2D O(4) spin model can be regarded as a superposition of two copies of XY-type graphs. The G space constructed by the configurations with two defects can be expressed as

$$G = \sum_{\mathcal{I} \neq \mathcal{M}} \vec{s}_{\mathcal{I}} \cdot \vec{s}_{\mathcal{M}} \exp(-\mathcal{H}) = \sum_{\alpha=1}^{2} G^{(\alpha)}(\mathcal{I}, \mathcal{M}),$$

$$G^{(\alpha)}(\mathcal{I}, \mathcal{M}) = \sum_{\{J^{\pm(1)}\}} \sum_{\{J^{\pm(2)}\}} \prod_{\langle ij \rangle} \left(\prod_{\beta=1}^{2} \frac{\left(K_{ij}^{(\beta)}/2\right)^{J_{ij}^{+(\beta)} + J_{ij}^{-(\beta)}}}{J_{ij}^{+(\beta)}! J_{ij}^{-(\beta)}!} \right) \prod_i \left(\frac{\prod_\beta \Gamma\left(\frac{\mathcal{J}_i^{(\beta)}+2}{2}\right)}{\Gamma\left(\frac{\sum_\beta \mathcal{J}_i^{(\beta)}+4}{2}\right)} \prod_{\beta=1}^{2} \delta\left(\sum_j \mathrm{sgn}(\boldsymbol{i} \to \boldsymbol{j}) \left(J_{ij}^{+(\beta)} - J_{ij}^{-(\beta)}\right) + \Delta_i^{(\alpha,\beta)} \right) \right), \tag{B6}$$

where $\Delta_i^{(\alpha,\beta)} = \delta(\alpha - \beta)(\delta(\boldsymbol{i} - \mathcal{I}) - \delta(\boldsymbol{i} - \mathcal{M}))$ and $\mathcal{J}_i^{(\beta)} = \sum_j (J_{ij}^{+(\beta)} + J_{ij}^{-(\beta)}) + \delta(\alpha - \beta)(\delta(\boldsymbol{i} - \mathcal{I}) + \delta(\boldsymbol{i} - \mathcal{M}))$. Since $\Delta_i^{(\alpha,\beta)}$ is nonzero when $\alpha = \beta$, two defects $\mathcal{I}, \mathcal{M}$ are only connected via an open path of one of the XY-type copies. The weight related to site $\boldsymbol{i}$ introduces the coupling of weights among two copies. The flow representation of the 2D O(4) spin model is shown in Fig. 7(b).

Given the flow configuration of O(4) spin model, we construct a bond percolation model by connecting nonzero flow variables $J^{\pm(\beta)}(\beta = 1, 2)$. For studying its percolation transition, we measure the wrapping probabilities R, R_e, and the mean size of the largest cluster per site

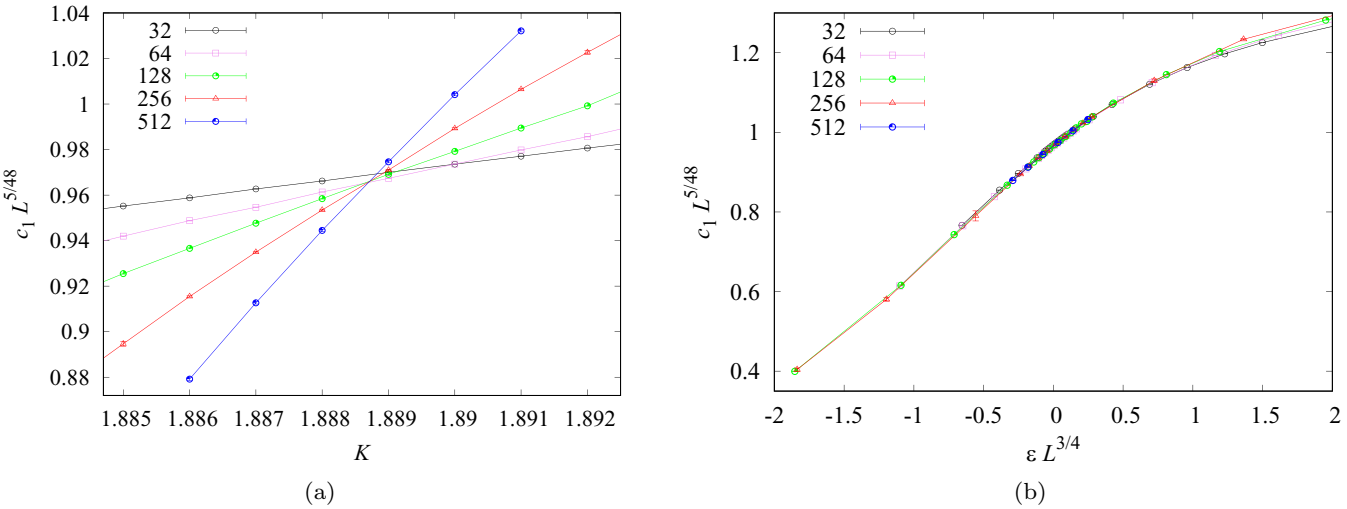

FIG. 10. Plots of $c_1 L^{5/48}$ vs K (a) and $c_1 L^{5/48}$ vs $\epsilon L^{3/4}$ (b) for different systems size L for the percolation model in the flow representation of the O(4) spin model. The solid lines connecting data points are added for clarity.

c_1. We find that this percolation transition indeed exists and should belong to the 2D percolation universality. Besides, critical polynomial $P_B(K, L) = R + R_e - 1$ is found to be equal to zero at $K = K_{\text{perc}}$ and $L \to \infty$, which is the same as the standard percolation model on the square lattice.

We estimate the percolation threshold K_{perc} by R and P_B. As shown in Fig. 9, $R^{(0)}$ and P_B curves for different system sizes have an intersection that quickly approaches to K_{perc} as $L \geqslant 64$. Around K_{perc}, we perform fits of the MC data for $R^{(0)}$ and P_B by the FSS ansatz

$$\mathcal{O}(\epsilon, L) = \mathcal{O}_c + \sum_{k=1}^{3} q_k \epsilon^k L^{k y_t} + b_1 L^{y_i}, \tag{B7}$$

where $\epsilon = K - K_{\text{perc}}$. We cannot obtain a stable estimate of y_i, so we fix $y_i = -2$, which is supported by wrapping probabilities of 2D percolation. In fact, the data for R_e and P_B can be well fitted with fixed $b_1 = 0$. The fitting results are summarized in Table V. We find that P_B at $K = K_{\text{perc}}$ is consistent with zero, and the estimate of $R_e = 0.690\,1(6)$ agrees with the exact universal value $R_e = 0.690\,473\,725$ [29,31]. We estimate $K_{\text{perc}} = 1.888\,70(6)$ and $y_t = 0.751(8)$.

Further, we study the mean size of the largest cluster per site for c_1 for different K and L. In Fig. 10(b), we plot $c_1 L^{5/48}$ versus $\epsilon L^{3/4}$, in which the collapse of curves confirms the scaling behavior $c_1 = L^{y_h - 2} \tilde{c}_1(\epsilon L^{y_t})$. It demonstrate that both the thermal exponent y_t and magnetic exponent y_h is consistent with the $y_t = 3/4$ and $y_h = 91/48$ for the standard percolation universality in two dimensions.

[1] V. L. Berezinsky, Destruction of long-range order in one-dimensional and two-dimensional systems possessing a continuous symmetry group. II. Quantum systems, Sov. Phys. JETP **34**, 610 (1972).
[2] J. M. Kosterlitz and D. J. Thouless, Long-range order and metastability in two-dimensional solids and superfluids (application of dislocation theory), J. Phys. C **5**, L124 (1972).
[3] J. M. Kosterlitz and D. J. Thouless, Ordering, metastability and phase transitions in two-dimensional systems, J. Phys. C **6**, 1181 (1973).
[4] J. M. Kosterlitz, The critical properties of the two-dimensional XY model, J. Phys. C **7**, 1046 (1974).
[5] M. E. Fisher, M. N. Barber, and D. Jasnow, Helicity modulus, superfluidity, and scaling in isotropic systems, Phys. Rev. A **8**, 1111 (1973).
[6] E. L. Pollock and D. M. Ceperley, Path-integral computation of superfluid densities, Phys. Rev. B **36**, 8343 (1987).
[7] D. R. Nelson and J. M. Kosterlitz, Universal Jump in the Superfluid Density of Two-Dimensional Superfluids, Phys. Rev. Lett. **39**, 1201 (1977).
[8] H. Weber and P. Minnhagen, Monte carlo determination of the critical temperature for the two-dimensional XY model, Phys. Rev. B **37**, 5986 (1988).
[9] N. Schultka and E. Manousakis, Finite-size scaling in two-dimensional superfluids, Phys. Rev. B **49**, 12071 (1994).
[10] P. Olsson, Monte Carlo analysis of the two-dimensional XY model. II. Comparison with the Kosterlitz renormalization-group equations, Phys. Rev. B **52**, 4526 (1995).
[11] M. Hasenbusch, The two-dimensional XY model at the transition temperature: A high-precision Monte Carlo study, J. Phys. A: Math. Gen. **38**, 5869 (2005).
[12] M. Hasenbusch, The binder cumulant at the Kosterlitz–Thouless transition, J. Stat. Mech.: Theory Exp. (2008) P08003.

[13] Y. Komura and Y. Okabe, Large-scale Monte Carlo simulation of two-dimensional classical XY model using multiple GPUs, J. Phys. Soc. Jpn. **81**, 113001 (2012).

[14] Y.-D. Hsieh, Y.-J. Kao, and A. W. Sandvik, Finite-size scaling method for the Berezinskii–Kosterlitz–Thouless transition, J. Stat. Mech.: Theory Exp. (2013) P09001.

[15] I. Dukovski, J. Machta, and L. V. Chayes, Invaded cluster simulations of the XY model in two and three dimensions, Phys. Rev. E **65**, 026702 (2002).

[16] H. Arisue, High-temperature expansion of the magnetic susceptibility and higher moments of the correlation function for the two-dimensional XY model, Phys. Rev. E **79**, 011107 (2009).

[17] L.-P. Arguin, Homology of Fortuin–Kasteleyn clusters of Potts models on the torus, J. Stat. Phys. **109**, 301 (2002).

[18] A. Morin-Duchesne and Y. Saint-Aubin, Critical exponents for the homology of Fortuin-Kasteleyn clusters on a torus, Phys. Rev. E **80**, 021130 (2009).

[19] Q. Liu, Y. Deng, T. M. Garoni, and H. W. J. Blöte, The o(n) loop model on a three-dimensional lattice, Nucl. Phys. B **859**, 107 (2012).

[20] T. Blanchard, Wrapping probabilities for Ising spin clusters on a torus, J. Phys. A: Math. Theor. **47**, 342002 (2014).

[21] H. Hu and Y. Deng, Universal critical wrapping probabilities in the canonical ensemble, Nucl. Phys. B **898**, 157 (2015).

[22] P. Hou, S. Fang, J. Wang, H. Hu, and Y. Deng, Geometric properties of the Fortuin-Kasteleyn representation of the Ising model, Phys. Rev. E **99**, 042150 (2019).

[23] C.-J. Huang, L. Liu, Y. Jiang, and Y. Deng, Worm-algorithm-type simulation of the quantum transverse-field Ising model, Phys. Rev. B **102**, 094101 (2020).

[24] M. E. J. Newman and R. M. Ziff, Efficient Monte Carlo Algorithm and High-Precision Results for Percolation, Phys. Rev. Lett. **85**, 4104 (2000).

[25] P. H. L. Martins and J. A. Plascak, Percolation on two- and three-dimensional lattices, Phys. Rev. E **67**, 046119 (2003).

[26] H. Hu, H. W. J. Blöte, and Y. Deng, Percolation in the canonical ensemble, J. Phys. A: Math. Theor. **45**, 494006 (2012).

[27] J. Wang, Z. Zhou, W. Zhang, T. M. Garoni, and Y. Deng, Bond and site percolation in three dimensions, Phys. Rev. E **87**, 052107 (2013).

[28] X. Xu, J. Wang, J.-P. Lv, and Y. Deng, Simultaneous analysis of three-dimensional percolation models, Front. Phys. **9**, 113 (2014).

[29] R. M. Ziff, C. D. Lorenz, and P. Kleban, Shape-dependent universality in percolation, Physica A **266**, 17 (1999).

[30] R. P. Langlands, C. Pichet, P. Pouliot, and Y. Saint-Aubin, On the universality of crossing probabilities in two-dimensional percolation, J. Stat. Phys. **67**, 553 (1992).

[31] H. T. Pinson, Critical percolation on the torus, J. Stat. Phys. **75**, 1167 (1994).

[32] X. Feng, Y. Deng, and H. W. J. Blöte, Percolation transitions in two dimensions, Phys. Rev. E **78**, 031136 (2008).

[33] Y. Wang, W. Guo, B. Nienhuis, and H. W. J. Blöte, Conducting-angle-based percolation in the XY model, Phys. Rev. E **81**, 031117 (2010).

[34] H. Hu, Y. Deng, and H. W. J. Blöte, Berezinskii-Kosterlitz-Thouless-like percolation transitions in the two-dimensional XY model, Phys. Rev. E **83**, 011124 (2011).

[35] N. Prokof'ev and B. Svistunov, Worm Algorithms for Classical Statistical Models, Phys. Rev. Lett. **87**, 160601 (2001).

[36] W. Xu, Y. Sun, J.-P. Lv, and Y. Deng, High-precision Monte Carlo study of several models in the three-dimensional U(1) universality class, Phys. Rev. B **100**, 064525 (2019).

[37] H. J. F. Knops, Exact Relation between the Solid-On-Solid Model and the XY Model, Phys. Rev. Lett. **39**, 766 (1977).

[38] L. N. Shchur and H. W. J. Blöte, Cluster Monte Carlo: T-scaling of systematic errors in the two-dimensional Ising model, Phys. Rev. E **55**, R4905(R) (1997).

[39] R. Kenna and A. C. Irving, The Kosterlitz-Thouless universality class, Nucl. Phys. B **485**, 583 (1997).

[40] W. Janke, Logarithmic corrections in the two-dimensional XY model, Phys. Rev. B **55**, 3580 (1997).

[41] J. F. Yu, Z. Y. Xie, Y. Meurice, Y. Liu, A. Denbleyker, H. Zou, M. P. Qin, J. Chen, and T. Xiang, Tensor renormalization group study of classical XY model on the square lattice, Phys. Rev. E **89**, 013308 (2014).

[42] L. Vanderstraeten, B. Vanhecke, A. M. Läuchli, and F. Verstraete, Approaching the Kosterlitz-Thouless transition for the classical XY model with tensor networks, Phys. Rev. E **100**, 062136 (2019).

[43] R. G. Jha, Critical analysis of two-dimensional classical XY model, J. Stat. Mech.: Theory Exp. (2020) 083203.

[44] D. J. Amit, Y. Y. Goldschmidt, and S. Grinstein, Renormalization group analysis of the phase transition in the 2D coulomb gas, sine-Gordon theory and XY-model, J. Phys. A: Math. Gen. **13**, 585 (1980).

[45] A. Pelissetto and E. Vicari, Renormalization-group flow and asymptotic behaviors at the Berezinskii-Kosterlitz-Thouless transitions, Phys. Rev. E **87**, 032105 (2013).

[46] N. V. Prokof'ev and B. V. Svistunov, Two definitions of superfluid density, Phys. Rev. B **61**, 11282 (2000).

[47] L. Zhang, M. Michel, E. M. Elçi, and Y. Deng, Loop-Cluster Coupling and Algorithm for Classical Statistical Models, Phys. Rev. Lett. **125**, 200603 (2020).

[48] L. Zhang, L. Liu, X. Tan, and Y. Deng, Dynamical critical behavior of worm algorithms for the o(n) spin model (unpublished).